Efficient toluene adsorption/desorption on biochar derived from in situ acid-treated sugarcane bagasse

Yuan Qu
Hubei Polytechnic University
Li Xu
Shanwei polutechnic
Yi Chen
Wuhan University of Science and Technology
Shikuan Sun
Foshan University
Yu Wang
Wuhan University of Science and Technology
Li Min Guo (lmguo@hust.edu.cn)
Huazhong University of Science and Technology - Main Campus: Huazhong University of Science and Technology https://orcid.org/0000-0002-6834-2758

Research Article

Keywords: hydrochar, VOCs, activated carbons, hydrothermal carbonization, sulfuric acid

Posted Date: April 7th, 2021

DOI: https://doi.org/10.21203/rs.3.rs-354810/v1

Version of Record: A version of this preprint was published at Environmental Science and Pollution Research on July 1st, 2021. See the published version at https://doi.org/10.1007/s11356-021-15128-2.

Efficient toluene adsorption/desorption on biochar derived from in situ acid-treated sugarcane bagasse

Yuan Qu[1], Li Xu[2,*], Yi Chen[3], Shikuan Sun[4], Yu Wang[3,**] and Limin Guo[5,***]

[1] School of Material Science and Engineering, Hubei Polytechnic University, Huangshi 435003, PR China

[2] Department of Ocean Engineering, Shanwei Polytechnic, Shanwei 516600, PR China

[3] College of Resources and Environmental Engineering, Wuhan University of Science and Technology, Wuhan 430081, PR China

[4] School of Material Science and Energy Engineering, Foshan University, Foshan, 528000, PR China

[5] School of Environmental Science and Technology, Huazhong University of Science and Technology, Wuhan, 430074, PR China

[*] Corresponding author

Email: xuli3021@gmail.com (L. Xu)

[**] Corresponding author

Email: yuwang@wust.edu.cn (Y. Wang)

[***] Corresponding author

Email: lmguo@hust.edu.cn (L. M. Guo)

Abstract

Carbon-based materials with great adsorption performance are of importance to meet the needs of industrial gas adsorption. Being massive agricultural wastes of sugarcane bagasse, China could use this waste into wealth. However, the comprehensive utilization of sugarcane bagasse as precursors for biochar that can be used as adsorbent has not been extensively explored. In this study, a series of in-situ sulfuric acid modified biochar were prepared by hydrothermal carbonization process. The prepared biochar (SBAC-7) is combined of two main advantages that are high microporosity (micropore surface area = 1106 m^2/g) and rich in S-containing functional groups on the surface. In particular, SBAC-7 showed an excellent adsorption capacity of toluene (771.1 mg/g) at 30 ^oC, which is nearly 3 times as high as the commercial activated carbons. Meanwhile, it showed great stability and cyclic regeneration performance with five toluene adsorption-desorption test cycles. This study provides a high-performance biochar for adsorption-desorption cycle in practical engineering applications, and would contribute to the sustainable "sugarcane production - bagasse utilization" circular economy.

Key words: hydrochar; VOCs; activated carbons; hydrothermal carbonization; sulfuric acid

1. Introduction

Volatile organic compounds (VOCs) are widely used in industries including petrochemicals, printing, pharmaceuticals and painting. VOCs are typical precursors in the atmospheric chemistry, contributing to the production of ozone, secondary organic aerosols, and greenhouse gases (He et al. 2019). In recent decades, various technologies for VOCs removal have been investigated, such as adsorption, membrane separation, catalytic combustion and photocatalytic degradation (Huang et al. 2020b, Li et al. 2020, Shu et al. 2019, Wang et al. 2020c, Wang et al. 2021). Among them, adsorption method has been considered as one of the most practical and effective technologies because of its low cost, easy operation and high treatment effects. Activated carbon (AC) is commonly used as adsorbents of VOCs because of their developed surface area and large pore volumes. However, traditional raw material like coal for AC preparation is non-renewable resources. And the main disadvantages of using these commercial AC materials for the VOCs adsorption are high production costs and secondary pollution during the preparation process.

Biochar derived from hydrothermal carbonization of carbohydrate-rich bio-resources was an ideal material for the purification of polluted water or air (Oliveira et al. 2019). Hydrothermal carbonization process could be directly applied to biomass with high moisture without predrying. Biochar has attracted many attention because of its potential in several crucial fields, such as catalysis, energy storage, CO_2 utilization and air purification (Wang et al. 2018a). Among the bio-resources, sugarcane bagasse (SB) with high carbon content, natural fibrous structure and huge amount of production is considered as an ideal precursor (Huang et al. 2020a). Sugarcane is a perennial C_4 crop cultivated in subtropical and tropical zones

worldwide. The high yields of lignocellulosic SB are considered as an excellent source for substituting fossil fuel as precursors. China is ranked in the third position in the world in sugarcane production (Huang et al. 2020a), however, the utilization of SB as precursors of biochar has not been extensively studied.

There is a growing consensus on modulating the functional group and internal textural structure, which play key factors in improving the adsorption performance of carbon-based material. The surface functional group can be modified by using various methods including acid/base treatment, chemical oxidation or impregnation with metal elements (Jin et al. 2020, Tang et al. 2020, Wang et al. 2020a). Notably, acid modification can change the surface alkalinity and oxygen-containing functional groups, which thus enhance the VOC selectivity and adsorption capacity (Kim et al. 2006, Tham et al. 2011, Vega et al. 2013b). Pak et al. reported that the AC treated by 10 vol% sulfuric acid showed a 47% increase in toluene adsorption capacity (Pak et al. 2016). Although these methods are effective to increase the oxygen-containing functional groups on the surface of AC, the specific surface area often decreases during the treatment process due to the block of internal textural structure. On the other hand, there are many other methods to modify activated carbon on internal textural structure, such as microwave modification, heat treatment modification, and hot steam treatment modification (Alslaibi et al. 2013). Based on the above studies, it is recognized that the adsorption capacity of biochar can be greatly enhanced by modulating the surface functional group and internal textural structure simultaneously.

Herein, we prepared a series of biochar by developing an in-situ acid-treated process using SB as bio-resources. Toluene, one of the typical VOCs, was chosen as the probe molecule to

evaluate the adsorptive properties of the as-prepared samples by the dynamic breakthrough experiments. The desorption property of in situ acid-treated biochar was also studied. This work is expected to expand the utilization of agricultural waste for air pollutant removal, plus a simple, low-cost, and efficient in-situ modification method.

2. Experimental

2.1 Raw materials

The original sugarcane bagasse (SB) was purchased form Guangxi Sugarcane Industry Research Institute (China), which was firstly pretreated by washing, drying and crushing into 0.6-0.8 mm. Sulfuric acid (H_2SO_4, 98 wt.%), potassium hydroxide (KOH, 85 wt.%), hydrochloric acid (HCl, 38 wt.%) and toluene (C_7H_8, 99.5 wt.%) were provided by Sinopharm Chemical Reagent Co., Ltd.

2.2 Sample preparation

Hydrothermal method was used to prepare activated carbon with deionized water or different concentrations of sulfuric acid solution (the concentration of sulfuric acid = 3, 5, 7, 9 wt.%). Typically, 3.0 g of the pretreated SB and 60 mL of deionized water or sulfuric acid solution were mixed into the reaction kettle and hydrothermal carbonization for 10 h at 240 °C. After cooling down naturally, the black samples were washed thoroughly with deionized water to neutral and dried at 105 °C overnight. And the carbonized product was obtained. Then, the carbonized product was impregnated with KOH solution (KOH/carbonized product weight ratio was 1.0) for 12 h. After drying at 105 °C for 12h, the impregnated samples were activated at 800 °C for 1 hour under N_2 flow, with a heating rate of 10 °C/min. After cooling down naturally, the samples were washed with HCl (10 wt.%) and deionized water until pH = 7 ±

0.05. Finally, the samples were dried at 105 °C for 12 h. The final products were denoted as SBAC-x (x = 0, 3, 5, 7, 9), x means the concentration of sulfuric acid solution.

2.3 Characterization

The crystalline phase of the samples was determined by X-ray diffraction (XRD, Rigaku/SmartLab SE), which was referred to International Centre for Diffraction Data (ICDD). The morphology was detected by scanning electron microscopy (SEM, ThermoFisher/Apreo S HiVac). The specific surface area, pore volume and pore diameter distribution were measured by N_2 adsorption-desorption isotherms at -196 °C using Micromeritics Tristar 3020. The specific surface area was calculated by using BET method according to nitrogen adsorption data in the relative pressure (P/P_0) range of 0.05-0.30. Sulfur, carbon and oxygen species in the samples were determined by X-ray photoelectron spectroscopy (XPS, AXIS SUPRA+) and Fourier transform infrared (FT-IR) spectra on a Bruker Tensor II spectrometer.

2.4 Toluene adsorption-desorption test

The toluene adsorption performance of SBAC-x was carried out by dynamic adsorption experiments at room temperature. The simulated exhaust gas consisted of 1,000 ppm toluene, 20% O_2 and N_2 as balance gas. 40 mg sample was weighed and put into a quartz tube, with quartz wool blocked on both sides. Before adsorption experiments, the sample was firstly degassed in 110 °C under N_2 flow to remove those adsorbed impurities. After cooling down to room temperature, the simulated exhaust gas was introduced to flow through the sample at a rate of 100 mL/min at a GHSV of 150,000 mL/(g·h). The tail gas from the reaction tube was led to the Gas Chromatograph (GC), and the concentration of toluene was noted every four minutes. The adsorption capacity was calculated through the integrals of the breakthrough

curve by using Eq. (1)

$$q_e = \frac{FMC_0}{22.4*m}\int_0^t \left(1-\frac{C_t}{C_0}\right) dt \quad (1)$$

where q_e (mg/g) is the calculated adsorption capacity, F (mL/min) is the gas flow rate, M (g/mol) is the relative molecular mass of adsorbate, C_0 (mg/mL) is the initial toluene concentration, C_t (mg/mL) is outlet toluene concentration at time t (min), m (g) is the mass of adsorbent used in the absorption experiment, and t (min) is the adsorption time.

In toluene desorption experiment, the temperature of the tested samples was elevated from 30 to 450 °C with a heating rate of 2.5 °C/min under 100 mL/min N_2. The toluene concentration of the effluent gas was measured by GC. Carbon balance (B_c) is calculated based on the peak areas of toluene desorption ($q_{\text{toluene}}^{\text{desorption}}$).

$$B_c(\%) = \frac{q_{\text{toluene}}^{\text{desorption}}}{q_e} \times 100\% \quad (2)$$

3. Results and discussion

3.1 Textural properties

XRD was carried out to investigate the crystallinity of SBAC-x as shown in **Fig. 1**. The as-prepared biochar showed broad peaks, indicating the amorphous structure (Gao et al. 2015). The broad peak in the range of 20-30° could be assigned to (002) plane of amorphous carbon. And the broad hump in the range of 40-50° was related to (100) plane, which were caused by diffusion scattering of the amorphous carbon (Chen et al. 2012, Cheng et al. 2020).

N_2 sorption isotherms and pore size distributions of the samples were depicted in **Fig. 2** and the textural properties were shown in **Table 1**. According to **Fig. 2a**, the sorption isotherm of SBAC-0 presented a hysteresis loop when the relative pressure $P/P_0 > 0.4$, which was associated with the capillary condensation of N_2. This phenomenon revealed that the untreated

SBAC-0 was rich in mesoporous channels (Wang et al. 2020b), and the surface area (S_{BET}) and total pore volume (V_t) of SBAC-0 was 1137 m^2/g and 0.76 cm^3/g, respectively. Notably, after the in situ sulfuric acid treatment, the S_{BET} and V_t of SBAC-x (x = 3, 5, 7, 9) were significantly enhanced. Specifically, the S_{BET} of SBAC-3, 5, 7 sharply increased to 2154, 2215 and 2455 m^2/g, while the V_t values increased to 1.24~1.26 cm^3/g, respectively (**Table 1**). These results may be attributed to the in-situ interaction between sulfuric acid and the fibers of sugarcane during the hydrothermal carbonization, which could provide more adsorption site for the adsorbate. The fibers of the sugarcane are composed of three major components (cellulose, hemicellulose and lignin), and it was reported that the hemicellulose can be removed by acid through etching effect (Huang et al. 2020a). Thus, both of the micropore surface area (1106 m^2/g) and the mesoporous surface area (1349 m^2/g) enlarged over the SBAC-7 sample than those of SBAC-0 under an appropriate concentration of sulfuric acid. When further increasing the sulfuric acid concentration to 9 wt.%, however, the micropore surface area of SBAC-9 decreased precipitously to 196 m^2/g, accompanied by the surge of mesoporous surface area (1926 m^2/g). This implies that the skeleton structure of sugarcane began to collapse under 9 wt.% sulfuric acid, resulting to the vanishment and blocking of micropores (Yang et al. 2020). The pore size distribution of the samples has a similar tendency with S_{BET} (**Fig. 2b**). It was recognized that the micropore played a decisive role in VOCs adsorption, especially when the VOCs concentration is low (Guo et al. 2020). Besides, the diffusion of VOC molecule is well situated to benefit from the presence of mesopores. Therefore, the SBAC-7 sample treated with the optimized acid concentration is better at keeping micropores and considerable amount of mesopores, which will own more excellent adsorption property.

The morphology of the as-prepared biochar was characterized by SEM as shown in **Fig. 3**. As shown in **Fig. 3a** and **b**, the SBAC-0 was in the shape of a fiber block with rough surface and few pores on the surface. After the hydrothermal carbonation in certain concentrations of sulfuric acid solution (i.e., 3~7 wt.%), the biochar could maintain the vascular bundle structure (**Fig. 3c** to **h**), which proved that the cage construction of SB precursor has a good corrosion resistance. However, when further increase the acid concentration to 9 wt.% (**Fig. 3i** and **j**), the pore diameter of SBAC-9 began to increase and the carbon skeleton was found to dilapidated and hollowed, which finally led to a decrease in micropore surface area (Wang et al. 2018b). This result is highly consistent with the N_2 sorption isotherms. In addition, the acid-treated SBAC-x have more smooth surface, which could be due to the cleaning effect of sulfuric acid solution for the surface impurities (Tang et al. 2016). Note that the etching between sulfuric acid and hemicellulose produced a lot of tiny pores on the surface, thus creating many interconnected channels perpendicular to the stems of SB. With elevating the sulfuric acid concentration, more external pores appeared (Jain et al. 2016), which was consistent with the increase of specific surface area of SBAC-x (**Table 1**).

3.2 Surface chemical properties

It had been reported that the type and number of chemical functional groups on the surface had great influence on adsorption performance. In order to explore the surface chemical functional group of as-prepared samples, FT-IR analysis was applied and presented in **Fig. 4**. The weak absorption peaks observed in the 3917-3539 cm^{-1} range and 672 cm^{-1} were assigned to the stretching vibration of dissociative O-H group. The spectra showed strong absorption peak at 3435 cm^{-1} represented the O-H stretching vibration in carboxyl and phenol (Pezoti et

188 al. 2016). The band located at 2362 cm^{-1} was attributed to the C=O stretching vibration, which
189 was due to carbon dioxide in the air. The peak located at 1721 cm^{-1} was related to the C=O
190 stretching vibration in aliphatic ketone, which appeared after the addition of sulfuric acid. The
191 band at 1630 and 1400 cm^{-1} correspond to the antisymmetric and symmetric stretching
192 vibrations of -COO- group. The bands located at 1120 cm^{-1} and 830 cm^{-1} were connected with
193 sulfur-containing functional groups, which was symmetrical stretching vibration of O=S=O
194 and C-O-S, respectively. And with the increase of sulfuric acid concentration, these two peaks
195 became more obvious. The peaks at 1581 and 1123 cm^{-1} were $-SO_2-$ and S=O stretching
196 vibration, which appeared while sulfuric acid concentration reached 7 wt.%. It could be easily
197 observed that the number of sulfur-containing functional groups increased with the increase of
198 sulfuric acid concentration. At the same time, the types and number of oxygen-containing
199 functional groups also increased, which might change the surface charge, hydrophilicity,
200 polarity and other surface chemical properties of the as-prepared biochar.

201 In order to further study the existing state of surface elements of activated carbons, XPS
202 analysis method was adopted and the results were shown in **Fig. 5** and **Table 2**. The survey
203 spectra of all the as-prepared activated carbons contain C 1s, O 1s and S 2p spectra. The sulfur
204 content of SBAC-0 was only 0.25%, which was due to the biological uptake by sugarcane
205 growth. After sulfuric acid treatment, the surface S content increased to some extent, which
206 indicated that the sulfur element had loaded on the surface of biochar during preparation.
207 Meanwhile, carbon content decreased and oxygen content increased with sulfuric acid
208 concentration increased. The XPS C 1s spectra of the samples shows three peaks at the binding
209 energies of 284.7, 286.3 and 289.3 eV, which were related to C-C, C-O and O=C-OH,

respectively (Cheng et al. 2020, Wang et al. 2019). The deconvoluted XPS S 2p signals at binding energies of 160.0, 164.3, 165.3 and 168.9 eV corresponded to functional groups such as S^{2-}, disulfide (C-S-S-C), sulfinyl group ($C_2S=O$), sulfone ($C_2S(=O_2)$) reported in previous studies (Grzybek et al. 2004, Ting et al. 2018). The XPS O 1s spectra，which were shown in **Fig. 5c**, can be disassembled into three peaks. The peak at the binding energies of 531.5 eV was ascribed to O=C of ketone, carbonyl and/or lactone groups. The band observed at 532.3 eV was assigned to C-O in ether and/or alcohol. And the peak located at 533.3 eV was corresponded to O=C-OH (Goel et al. 2015, Guo et al. 2020). It is believed that O=C and C-O were responsible for surface basicity and O=C-OH reflected the surface acidity (Tiwari et al. 2018). The surface adsorption active sites of biochar were related to the surface functional group as mentioned above (Vega et al. 2013a). The amount and proportion of surface basicity increased with the rose of sulfuric acid concentration, which lead to a rise in pH_{pzc} of zero potential point on the surface, thus enhancing the non-polarity of the activated carbon. Additionally, toluene was a weak or non-polar molecule. The increased surface basicity can promote the adsorption capacity of toluene by increasing the π-π electron diffusion capability on the biochar.

3.3 Adsorption capacity of the biochar

The dynamic adsorption behaviors of toluene on different samples were considered and the breakthrough curves were presented in **Fig. 6**. The corresponding saturated adsorption capacity was 387.6, 641.4, 695.0, 771.7 and 711.8 mg/g from 0 to 9 wt.% of sulfuric acid, respectively. Apparently, above results agreed with the textural properties (specific surface area and pore properties) and surface functionalities (amount and proportion of surface groups). Besides,

breakthrough time was defined as the time when outlet toluene concentration reached 1% of feed concentration, which was more commonly used in practical applications. For the SBAC-x samples, the breakthrough time was 16, 44, 60, 68 and 60 min, respectively. As is known, the adsorption capacity of commercial activated carbon is usually at 200 to 300 mg/g, which is only one third of our best sample (SBAC-7). **Table 3** compared the toluene adsorption capacity of the as-prepared SBAC-7 with those of other carbon-based adsorbent reported in the literature, which also indicate the excellent adsorption capacity of SBAC-7 in this work. As described in **Fig. 2** and **Table 1**, the specific surface area and ratio of micropore reaches the maximum value when sulfuric acid was added at 7 wt.%. Meanwhile, the carbon skeleton and surface structure were the most abundant. In addition, as shown in **Fig. 5** and **Table 2**, the addition of sulfuric acid enhanced the surface basicity. These suggest that the pore structure and surface functional groups are the core factors to improve the adsorption capacity of biochar for toluene.

Although the adsorption capacity of adsorbent is important, the desorption capacity which determine the regeneration effect is also noteworthy. The common method of desorption is treatment in high temperature with N_2 or water vapour, which means that the lower temperature and higher desorption efficiency could reduce energy consumption as much as possible. In order to understand the regeneration process, desorption test of SBAC-0 and SBAC-7 was compared and the result was shown in **Fig. 7**. On both samples the desorption peak appeared at 90 °C, which was much lower than the previously reported 110 °C (Zhu et al. 2020). Moreover, the carbon balance of SBAC-7 (ca. 98.7%) was much higher than SBAC-0 (ca. 73.6%). This may be explained by the existence of mesopores which promoted toluene transfer and suitable adsorption strength due to the huge amount of S-containing functional groups.

Considering the stability of the SBAC-7 sample, adsorption-desorption cycle test was performed as shown in **Fig. 8**. The regeneration temperature in each cycle was set at 90 °C according to the desorption test. It was found that the breakthrough time of SBAC-7 did not change remarkably during the five cycles. The saturation adsorption capacity was 771.7, 759.7, 753.3, 748.8 and 742.3 mg/g, respectively. The last adsorption capacity only decreased by 3.8% compare that to the first time. Analysis of the reactor effluent at the desorption steps during the five cycles confirmed that the toluene was desorbed completely. This is proved by the excellent carbon balances obtained during cycling (>96%). These results imply that SBAC-7 was renewable, reusable and recyclable during the adsorption-desorption cycle.

3.4 Adsorption kinetics model

To further understand the adsorption mechanism of toluene on as-prepared samples, four common models including quasi-first-order, quasi-second-order, Elovich and Bangham kinetic models were used to fit the experimental data (Tang et al. 2016, Zhang et al. 2019). The models were detail described as follows.

(1) Pseudo-first order model

$$q_t = q_e(1 - e^{-k_1 t}) \quad (3)$$

where q_t and q_e was the amount of toluene adsorption at time t and equilibrium (mg/g), and k_1 was the quasi-second-order rate constant (min^{-1}).

(2) Pseudo-second order model

$$q_t = \frac{k_2 {q_e}^2 t}{1 + k_2 q_e t} \quad (4)$$

where k_2 is the quasi-second-order rate constant (min^{-1}).

(3) Elovich model

$$q_t = \frac{\ln(\alpha\beta)+lnt}{\beta} \quad (5)$$

Where α is the initial adsorption rate constant (mg g^{-1} min^{-1}) and β is the desorption rate constant (g/mg).

(4) Bangham model

$$q_t = q_e - \frac{q_e}{e^{kt^z}} \quad (6)$$

where k is the Bangham constant (min^{-1}) and z is a constant.

The fitting curve and estimated parameters are shown in **Fig. 9** and **Table 4**. It can be easily found that only the Bangham model was well fitting and the correlation coefficients (R_2) were <0.99. Meanwhile, the adsorption capacity predicted by this model was closer to the actual measured value, from which we can conclude that the Bangham model was the best model for toluene adsorption in as-prepared samples. It revealed that toluene adsorption involved two parts: toluene adsorption at the surface and diffusion in the pores (Lei et al. 2020). Moreover, the intraparticle diffusion played a major role, which could affect the adsorption rate (Gong et al. 2019).

4. Conclusions

In short, we presented a facile in-situ modification method for biochar with excellent performance. The as-prepared biochar owned high specific surface areas, great pore volumes and abundant surface chemical group. SBAC-7 exhibited the best toluene adsorption capacity of 771.7 mg/g, which was about 3 times higher than that of commercial ACs, while retaining mild flexibility. Meanwhile, it showed considerable stability and cyclic regeneration performance with five toluene adsorption-desorption test cycles. The outstanding performance was associated with its superior physicochemical properties. On one hand, etching effect of

sulfuric acid were conducive to higher specific surface area (2245 m^2/g) and formation of more micropores. Others, the surface S-containing functional groups surged by adding sulfuric acid, which enhancing the surface basicity and non-polarity of the biochar. These factors simultaneously promoted the adsorption and internal diffusion of toluene molecule. This work provided a valuable guide to produce applicable adsorbents with agricultural wastes for the adsorption of toluene in the practical implications.

Acknowledgments

The present work is supported by Scientific Research Program Guidance Project of Hubei Province (No. B2020210) and Natural Science Foundation of Hubei Province (2019CFA070).

Conflict of interest

The authors declare that they have no conflict of interests.

Ethical approval

The article is original. The manuscript has not been published previously by any of the authors, is not under consideration for publication in any other journal at the time of submission, will not be submitted elsewhere before one decision is made. No conflict of interest exists. If accepted, the article will not be published elsewhere in the same form, in any language, without the written consent of the publisher.

Consent to participate

All authors have participated in the study works.

Consent to publish

All authors are aware of the submission and agree to its publication.

Authors Contributions

Li Xu, Yu Wang and Limin Guo conceived and designed the experiments. Yuan Qu and Yi Chen carried out materials syntheses. Yuan Qu, Yi Chen and Shikuan Sun performed all activity tests and related measurements and interpretation of results. Yuan Qu amd Yi Chen performed the original draft. All authors discussed the results and edited the manuscript. All authors reviewed and approved the manuscript. Limin Guo supervised the study.

Funding

The present work is funded by Scientific Research Program Guidance Project of Hubei Province (No. B2020210) and Natural Science Foundation of Hubei Province (2019CFA070).

Data availability

All data generated or analyzed during this study are included in this published article.

References

Alslaibi TM, Abustan I, Ahmad MA, Foul AA (2013): A review: production of activated carbon from agricultural byproducts via conventional and microwave heating. Journal of Chemical Technology & Biotechnology 88, 1183-1190

Chen H, Wang H, Xue Z, Yang L, Xiao Y, Zheng M, Lei B, Liu Y, Sun L (2012): High hydrogen storage capacity of rice hull based porous carbon. Int. J. Hydrogen Energy 37, 18888-18894

Cheng H, Sun Y, Wang X, Zou S, Ye G, Huang H, Ye D (2020): Hierarchical porous carbon fabricated from cellulose-degrading fungus modified rice husks: Ultrahigh surface area and impressive improvement in toluene adsorption. J. Hazard. Mater. 392, 122298

Gao Y, Li L, Jin Y, Wang Y, Yuan C, Wei Y, Chen G, Ge J, Lu H (2015): Porous carbon made from rice husk as electrode material for electrochemical double layer capacitor. Appl.

342 Energy 153, 41-47
343 Goel C, Bhunia H, Bajpai PK (2015): Synthesis of nitrogen doped mesoporous carbons for
344 carbon dioxide capture. RSC Advances 5, 46568-46582
345 Gong H, Liu W, Liu L, Goyal N, Xiao P, Li G, Wei Y, Du T (2019): In-situ synthesis of an
346 excellent CO2 capture material chabazite. J. Taiwan Inst. Chem. Eng. 103, 160-166
347 Grzybek T, Pietrzak R, Wachowska H (2004): The Comparison of Oxygen and Sulfur Species
348 Formed by Coal Oxidation with O2/Na2CO3or Peroxyacetic Acid Solution. XPS
349 Studies. Energy & fuels 18, 804-809
350 Guo Y, Tan C, Sun J, Li W, Zhang J, Zhao C (2020): Porous activated carbons derived from
351 waste sugarcane bagasse for CO2 adsorption. Chem. Eng. J. 381, 122736
352 He C, Cheng J, Zhang X, Douthwaite M, Pattisson S, Hao Z (2019): Recent Advances in the
353 Catalytic Oxidation of Volatile Organic Compounds: A Review Based on Pollutant
354 Sorts and Sources. Chem. Rev. 119, 4471-4568
355 Hossein Tehrani NHM, Alivand MS, Rashidi A, Rahbar Shamskar K, Samipoorgiri M, Esrafili
356 MD, Mohammady Maklavany D, Shafiei-Alavijeh M (2020): Preparation and
357 characterization of a new waste-derived mesoporous carbon structure for ultrahigh
358 adsorption of benzene and toluene at ambient conditions. J Hazard Mater 384, 121317
359 Hu L, Peng Y, Wu F, Peng S, Li J, Liu Z (2017): Tubular activated carbons made from cotton
360 stalk for dynamic adsorption of airborne toluene. J. Taiwan Inst. Chem. Eng. 80, 399-
361 405
362 Huang J, Khan MT, Perecin D, Coelho ST, Zhang M (2020a): Sugarcane for bioethanol
363 production: Potential of bagasse in Chinese perspective. Renewable Sustainable Energy

364 Rev. 133, 110296
365 Huang S, Deng W, Zhang L, Yang D, Gao Q, Tian Z, Guo L, Ishihara T (2020b): Adsorptive
366 properties in toluene removal over hierarchical zeolites. Microporous Mesoporous
367 Mater. 302, 110204
368 Jain A, Balasubramanian R, Srinivasan MP (2016): Hydrothermal conversion of biomass waste
369 to activated carbon with high porosity: A review. Chem. Eng. J. 283, 789-805
370 Jin Z, Wang B, Ma L, Fu P, Xie L, Jiang X, Jiang W (2020): Air pre-oxidation induced high
371 yield N-doped porous biochar for improving toluene adsorption. Chem. Eng. J. 385,
372 123843
373 Kim K-J, Kang C-S, You Y-J, Chung M-C, Woo M-W, Jeong W-J, Park N-C, Ahn H-G (2006):
374 Adsorption–desorption characteristics of VOCs over impregnated activated carbons.
375 Catal. Today 111, 223-228
376 Lei B, Liu B, Zhang H, Yan L, Xie H, Zhou G (2020): CuO-modified activated carbon for the
377 improvement of toluene removal in air. Journal of Environmental Sciences 88, 122-132
378 Li X, Zhang L, Yang Z, Wang P, Yan Y, Ran J (2020): Adsorption materials for volatile organic
379 compounds (VOCs) and the key factors for VOCs adsorption process: A review. Sep.
380 Purif. Technol. 235, 116213
381 Oliveira JA, Cunha FA, Ruotolo LAM (2019): Synthesis of zeolite from sugarcane bagasse fly
382 ash and its application as a low-cost adsorbent to remove heavy metals. Journal of
383 Cleaner Production 229, 956-963
384 Pak S-H, Jeon M-J, Jeon Y-W (2016): Study of sulfuric acid treatment of activated carbon used
385 to enhance mixed VOC removal. International Biodeterioration & Biodegradation 113,

195-200

Pezoti O, Cazetta AL, Bedin KC, Souza LS, Martins AC, Silva TL, Santos Júnior OO, Visentainer JV, Almeida VC (2016): NaOH-activated carbon of high surface area produced from guava seeds as a high-efficiency adsorbent for amoxicillin removal: Kinetic, isotherm and thermodynamic studies. Chem. Eng. J. 288, 778-788

Qie Z, Sun F, Zhang Z, Pi X, Qu Z, Gao J, Zhao G (2020): A facile trace potassium assisted catalytic activation strategy regulating pore topology of activated coke for combined removal of toluene/SO2/NO. Chem. Eng. J. 389, 124262

Shen Y, Zhang N (2019): Facile synthesis of porous carbons from silica-rich rice husk char for volatile organic compounds (VOCs) sorption. Bioresource Technology 282, 294-300

Shi X, Zhang X, Bi F, Zheng Z, Sheng L, Xu J, Wang Z, Yang Y (2020): Effective toluene adsorption over defective UiO-66-NH2: An experimental and computational exploration. J. Mol. Liq. 316, 113812

Shu Y, He M, Ji J, Huang H, Liu S, Leung DYC (2019): Synergetic degradation of VOCs by vacuum ultraviolet photolysis and catalytic ozonation over Mn-xCe/ZSM-5. J. Hazard. Mater. 364, 770-779

Tang L, Li L, Chen R, Wang C, Ma W, Ma X (2016): Adsorption of acetone and isopropanol on organic acid modified activated carbons. Journal of Environmental Chemical Engineering 4, 2045-2051

Tang M, Huang X, Peng Y, Lu S (2020): Hierarchical porous carbon as a highly efficient adsorbent for toluene and benzene. Fuel 270, 117478

Tham YJ, Latif PA, Abdullah AM, Shamala-Devi A, Taufiq-Yap YH (2011): Performances of

toluene removal by activated carbon derived from durian shell. Bioresource Technology 102, 724-728

Ting Y, Chen C, Ch'ng B-L, Wang Y-L, Hsi H-C (2018): Using raw and sulfur-impregnated activated carbon as active cap for leaching inhibition of mercury and methylmercury from contaminated sediment. J Hazard Mater 354, 116-124

Tiwari D, Bhunia H, Bajpai PK (2018): Adsorption of CO2 on KOH activated, N-enriched carbon derived from urea formaldehyde resin: kinetics, isotherm and thermodynamic studies. Appl. Surf. Sci. 439, 760-771

Vega E, Lemus J, Anfruns A, Gonzalez-Olmos R, Palomar J, Martin MJ (2013a): Adsorption of volatile sulphur compounds onto modified activated carbons: effect of oxygen functional groups. J. Hazard. Mater. 258-259, 77-83

Vega E, Lemus J, Anfruns A, Gonzalez-Olmos R, Palomar J, Martin MJ (2013b): Adsorption of volatile sulphur compounds onto modified activated carbons: Effect of oxygen functional groups. J Hazard Mater 258-259, 77-83

Wang S, Nam H, Nam H (2020a): Preparation of activated carbon from peanut shell with KOH activation and its application for H2S adsorption in confined space. Journal of Environmental Chemical Engineering 8, 103683

Wang T, Zhai Y, Zhu Y, Li C, Zeng G (2018a): A review of the hydrothermal carbonization of biomass waste for hydrochar formation: Process conditions, fundamentals, and physicochemical properties. Renewable Sustainable Energy Rev. 90, 223-247

Wang T, Zhu J, Wei Z, Yang H, Ma Z, Ma R, Zhou J, Yang Y, Peng L, Fei H, Lu B, Duan X (2019): Bacteria-Derived Biological Carbon Building Robust Li-S Batteries. Nano Lett.

19, 4384-4390

Wang Y, Yang D, Li S, Chen M, Guo L, Zhou J (2018b): Ru/hierarchical HZSM-5 zeolite as efficient bi-functional adsorbent/catalyst for bulky aromatic VOCs elimination. Microporous Mesoporous Mater. 258, 17-25

Wang Y, Chen Y, Zhang L, Wang G, Deng W, Guo L (2020b): Total catalytic oxidation of chlorinated aromatics over bimetallic Pt–Ru supported on hierarchical HZSM-5 zeolite. Microporous Mesoporous Mater. 308, 110538

Wang Y, Liu K, Wu J, Hu Z, Huang L, Zhou J, Ishihara T, Guo L (2020c): Unveiling the Effects of Alkali Metal Ions Intercalated in Layered MnO2 for Formaldehyde Catalytic Oxidation. ACS Catal. 10, 10021-10031

Wang Y, Wu J, Wang G, Yang D, Ishihara T, Guo L (2021): Oxygen Vacancy Engineering in Fe Doped Akhtenskite-Type MnO2 for Low-Temperature Toluene Oxidation. Appl. Catal. B: Environ. 285, 119873

Yang D, Fu S, Huang S, Deng W, Wang Y, Guo L, Ishihara T (2020): The preparation of hierarchical Pt/ZSM-5 catalysts and their performance for toluene catalytic combustion. Microporous Mesoporous Mater. 296, 109802

Zhang X, Gao B, Fang J, Zou W, Dong L, Cao C, Zhang J, Li Y, Wang H (2019): Chemically activated hydrochar as an effective adsorbent for volatile organic compounds (VOCs). Chemosphere (Oxford) 218, 680-686

Zhao X, Zeng X, Qin Y, Li X, Zhu T, Tang X (2018): An experimental and theoretical study of the adsorption removal of toluene and chlorobenzene on coconut shell derived carbon. Chemosphere 206, 285-292

452 Zhou K, Ma W, Zeng Z, Ma X, Xu X, Guo Y, Li H, Li L (2019): Experimental and DFT study
453 on the adsorption of VOCs on activated carbon/metal oxides composites. Chem. Eng.
454 J. 372, 1122-1133
455 Zhu J, Li Y, Xu L, Liu Z (2018): Removal of toluene from waste gas by adsorption-desorption
456 process using corncob-based activated carbons as adsorbents. Ecotoxicology and
457 Environmental Safety 165, 115-125
458 Zhu L, Shen D, Luo KH (2020): A critical review on VOCs adsorption by different porous
459 materials: Species, mechanisms and modification methods. J. Hazard. Mater. 389,
460 122102
461
462

Figure captions

Figure 1. XRD patterns of the as-prepared samples.

Figure 2. (a) N_2 sorption isotherms and (b) pore-size distributions of the as-prepared samples.

Figure 3. SEM images of as-prepared activated carbon samples SBAC-0 (a, b), SBAC-3 (c, d), SBAC-5 (e, f), SBAC-7 (g, h), and SBAC-9 (i, j).

Figure 4. FT-IR spectra of the as-prepared samples.

Figure 5. (a) C 1s, (b) S 2p and (c) O 1s XPS spectra of the as-prepared samples.

Figure 6. Adsorption breakthrough curves of as-prepared samples.

Figure 7. Desorption curves of SBAC-0 (a) and SBAC-7 (b).

Figure 8. The consecutive toluene adsorption-desorption cycles of SBAC-7.

Figure 9. Adsorption kinetics model fit adsorption curve: (a) Pseudo-first-order model, (b) Pseudo-second-order model, (c) Elovich model, (d) Bangham model.

Tables

Table 1. BET surface areas and pore volumes of the as-prepared samples.

Samples	S_{BET}[a] (m^2/g)	S_{mic}[b] (m^2/g)	S_{mes} (m^2/g)	V_t[c] (cm^3/g)	V_{mic}[b] (cm^3/g)	V_{mes} (cm^3/g)
SBAC-0	1137	929	208	0.76	0.48	0.28
SBAC-3	2154	768	1386	1.24	0.43	0.81
SBAC-5	2215	636	1579	1.24	0.36	0.88
SBAC-7	2455	1106	1349	1.26	0.53	0.73
SBAC-9	2122	196	1926	1.28	0.12	1.16

[a] Specific surface area calculated by BET method at P/P_0=0.05-0.30.

[b] Micropore evaluated by t-plot method.

[c] Total pore volume obtained from the single point adsorption volume at P/P_0=0.995.

485 **Table 2**. Quantitative characterization of the surface compositions of the as-prepared samples.

Samples	Surface atomic (%)			Peak area ratio (%)		
	C 1s	S 2p	O 1s	C=O/O1s	C-O/O1s	COOH/O1s
SBAC-0	95.33	0.25	4.42	12.47	28.27	59.26
SBAC-3	94.96	0.42	4.62	3.12	42.91	53.97
SBAC-5	94.61	1.18	4.21	5.42	43.06	51.52
SBAC-7	90.25	2.71	7.04	33.04	25.76	41.20
SBAC-9	86.23	2.56	11.21	26.51	37.12	36.37

486

Table 3. Toluene adsorption capacity reported in the literature.

Materials	Experiment conditions	S_{BET} (m^2/g)	Adsorption capacity (mg/g)	Breakthrough time (min)	Reference
10S-AC	150 ppm, 6 L min^{-1}, room temperature	840	123	240	(Pak et al. 2016)
Commercial AC	10.0 g m^{-3}, 50 mL min^{-1}, 298 K	934	41	100	(Zhou et al. 2019)
AC/MgO	10.0 g m^{-3}, 50 mL min^{-1}, 298 K	794	56	110	(Zhou et al. 2019)
AC/ZnO	10.0 g m^{-3}, 50 mL min^{-1}, 298 K	847	68	130	(Zhou et al. 2019)
AC/CuO	10.0 g m^{-3}, 50 mL min^{-1}, 298 K	769	46	130	(Zhou et al. 2019)
AC/ZrO_2	10.0 g m^{-3}, 50 mL min^{-1}, 298 K	837	127	120	(Zhou et al. 2019)
AC (rice husk)	300 ppm, 30 mL min^{-1}, 293 K	1818	264	2784	(Shen &Zhang 2019)
CBAC-1.0-1.0-550	3000 mg m^{-3}, 500 ml min^{-1}, 298 K	1501	414.6	72	(Zhu et al. 2018)
AC (petroleum waste)	10%, 125 mL min^{-1}, 298 K	2692	659.9	65	(Hossein Tehrani et al. 2020)
CAC	80 ppm, 2 L min^{-1}, 303 K	1011	189	348	(Zhao et al. 2018)
CDC	80 ppm, 2 L min^{-1}, 303 K	1137	255	544	(Zhao et al. 2018)
UiO-66-NH2	1000 ppm, 50 mL min^{-1}, 298K	568	162	148	(Shi et al. 2020)
C-U-N-0.5	1000 ppm, 50 mL min^{-1}, 298K	795	228	228	(Shi et al. 2020)
BP (350/120/2)	600 ppmv, 120 mL min^{-1}, 303K	762.9	352.7	282	(Jin et al. 2020)
KP-AC-2	190 ppmv, 250 mL min^{-1}, 298K	1283.6	300.3	200	(Qie et al. 2020)
AC-P	1000 ppm, 150 mL min^{-1}, 298K	1256	328	300	(Hu et al. 2017)
AC-Z	1000 ppm, 150 mL min^{-1}, 298K	795	258	300	(Hu et al. 2017)
NHPC-900	600 ppm, 200 mL min^{-1}, 303K	778	272	54	(Tang et al. 2020)
HPC-900	600 ppm, 200 mL min^{-1}, 303K	578	182	36	(Tang et al. 2020)
SBAC-7	1000 ppm, 100 mL min^{-1}, 303K	2455	771.7	80	This work

Table 4. Adsorption kinetics fitting parameters of toluene adsorption on as-prepared samples.

Samples	Pseudo-first order model		Pseudo-second order model		Elovich model			Bangham model			q_e (mg/g)
	k_1	R^2	k_2	R^2	α	β	R^2	k	z	R^2	
SBAC-0	0.0945	0.911	$5.32*10^{-5}$	0.939	37.196	$7.96*10^{-3}$	0.948	$1.16*10^{-2}$	1.397	0.999	387.6
SBAC-3	0.0766	0.867	$4.39*10^{-6}$	0.754	38.191	$4.21*10^{-3}$	0.939	$4.19*10^{-3}$	1.484	0.996	641.4
SBAC-5	0.0753	0.881	$1.87*10^{-6}$	0.635	38.960	$3.81*10^{-3}$	0.921	$3.13*10^{-3}$	1.529	0.993	695.0
SBAC-7	0.0741	0.763	$1.85*10^{-6}$	0.620	39.527	$3.46*10^{-3}$	0.905	$3.3*10^{-3}$	1.442	0.993	771.7
SBAC-9	0.0773	0.851	$4.44*10^{-7}$	0.523	39.051	$3.73*10^{-3}$	0.919	$3.22*10^{-3}$	1.505	0.993	711.8

Figure 1

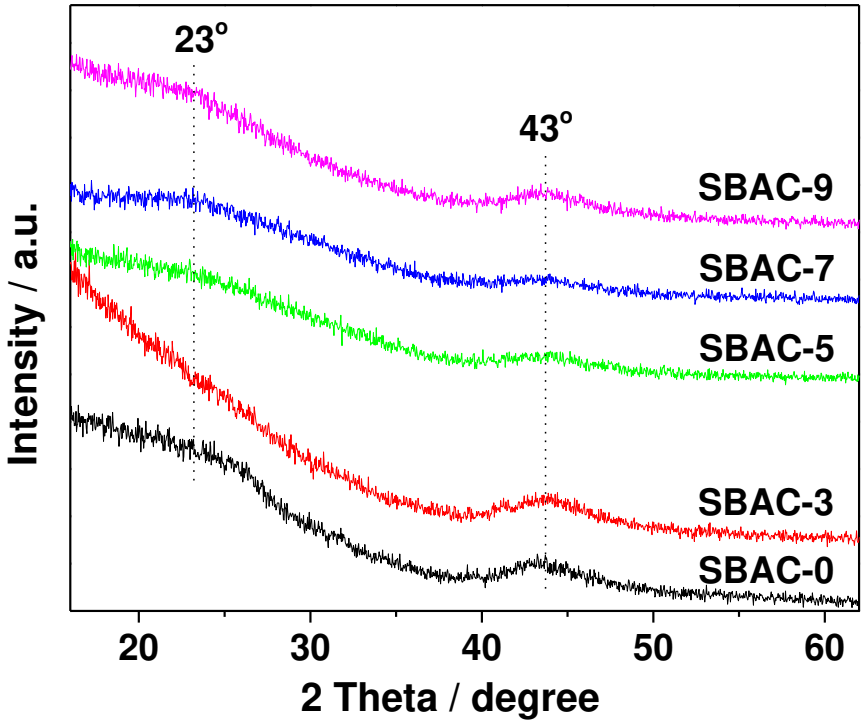
23°
43°
SBAC-9
SBAC-7
SBAC-5
SBAC-3
SBAC-0
Intensity / a.u.
20
30
40
50
60
2 Theta / degree

Figure 2

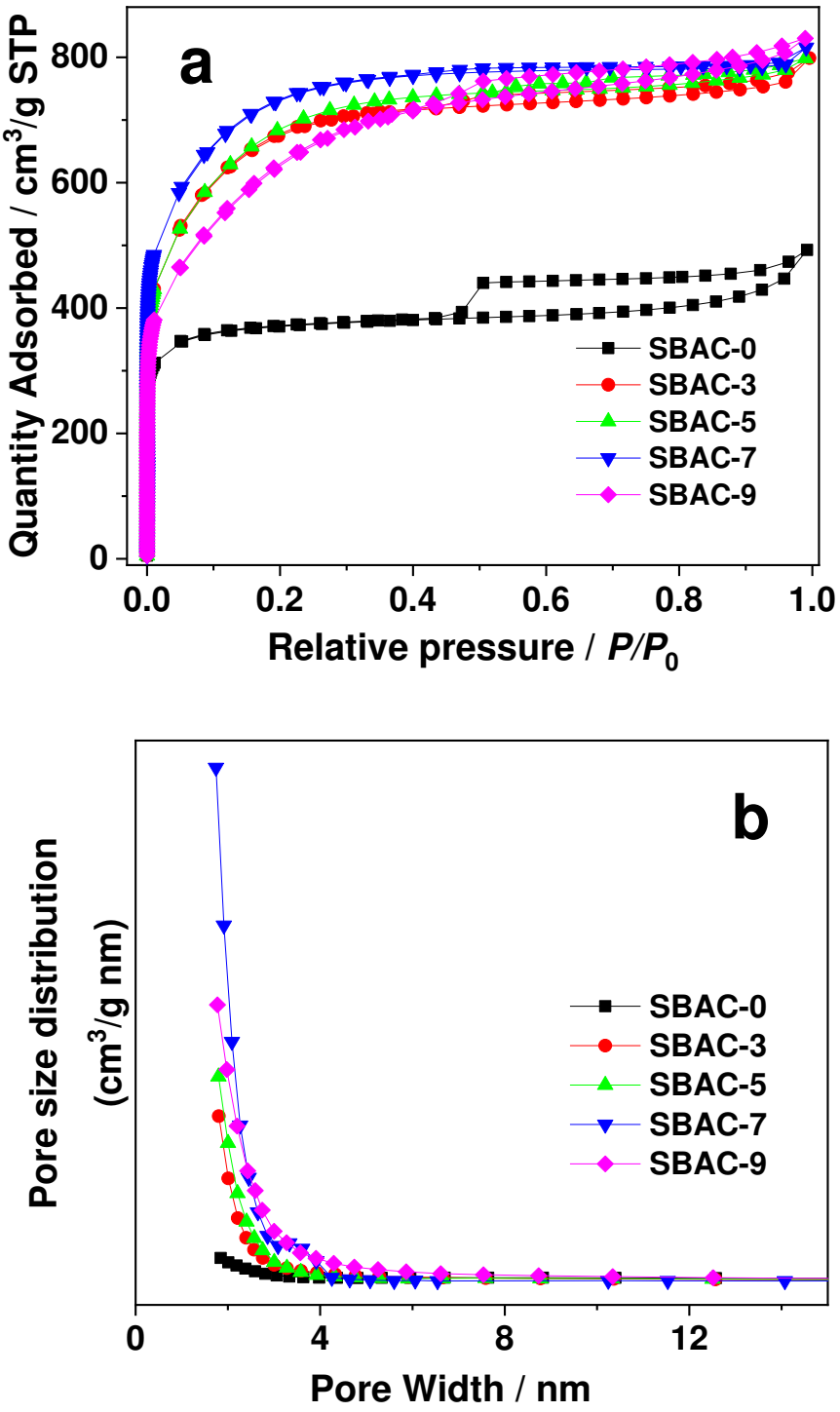
a
Quantity Adsorbed / cm3/g STP
0
200
400
600
800
0.0
0.2
0.4
0.6
0.8
1.0
Relative pressure / P/P0
SBAC-0
SBAC-3
SBAC-5
SBAC-7
SBAC-9
b
Pore size distribution
(cm3/g nm)
0
4
8
12
Pore Width / nm
SBAC-0
SBAC-3
SBAC-5
SBAC-7
SBAC-9

Figure 3

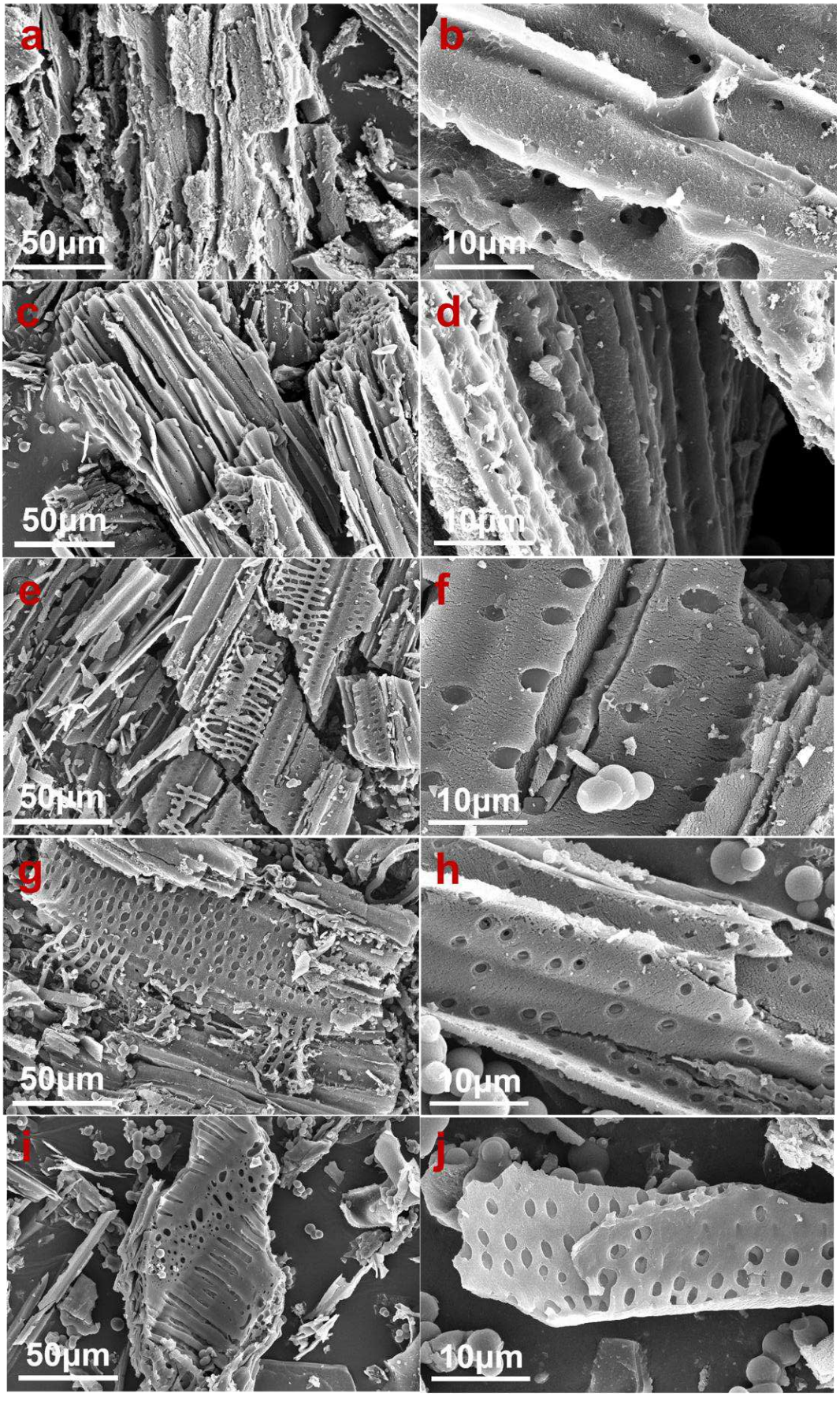
a
50μm
b
10μm
c
50μm
d
10μm
e
50μm
f
10μm
g
50μm
h
10μm
i
50μm
j
10μm

Figure 4

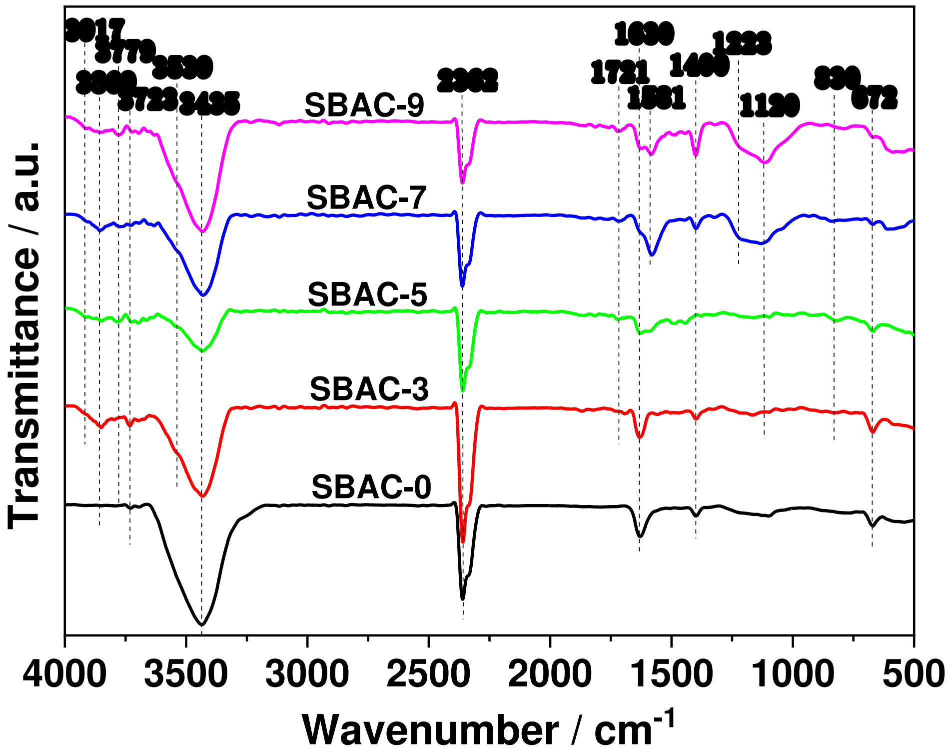
3917
3779
3530
3723
3435
2362
1630
1721
1400
1223
1120
672
SBAC-9
SBAC-7
SBAC-5
SBAC-3
SBAC-0
Transmittance / a.u.
4000
3500
3000
2500
2000
1500
1000
500
Wavenumber / cm-1

Figure 5

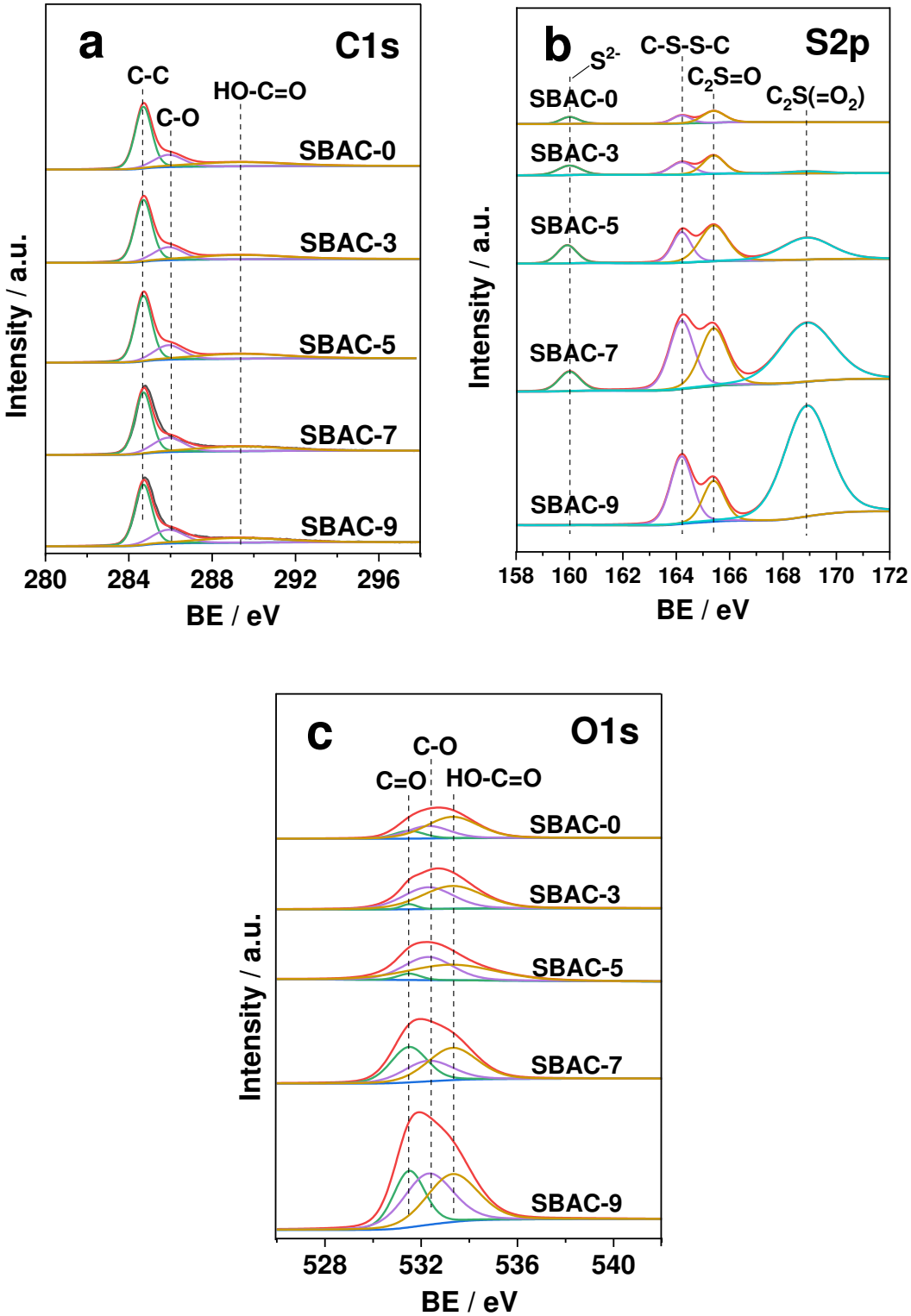
a
C1s
C-C
C-O
HO-C=O
SBAC-0
SBAC-3
SBAC-5
SBAC-7
SBAC-9
Intensity / a.u.
280
284
288
292
296
BE / eV
b
S2p
S2-
C-S-S-C
C2S=O
C2S(=O2)
SBAC-0
SBAC-3
SBAC-5
SBAC-7
SBAC-9
Intensity / a.u.
158
160
162
164
166
168
170
172
BE / eV
c
O1s
C-O
C=O
HO-C=O
SBAC-0
SBAC-3
SBAC-5
SBAC-7
SBAC-9
Intensity / a.u.
528
532
536
540
BE / eV

Figure 6

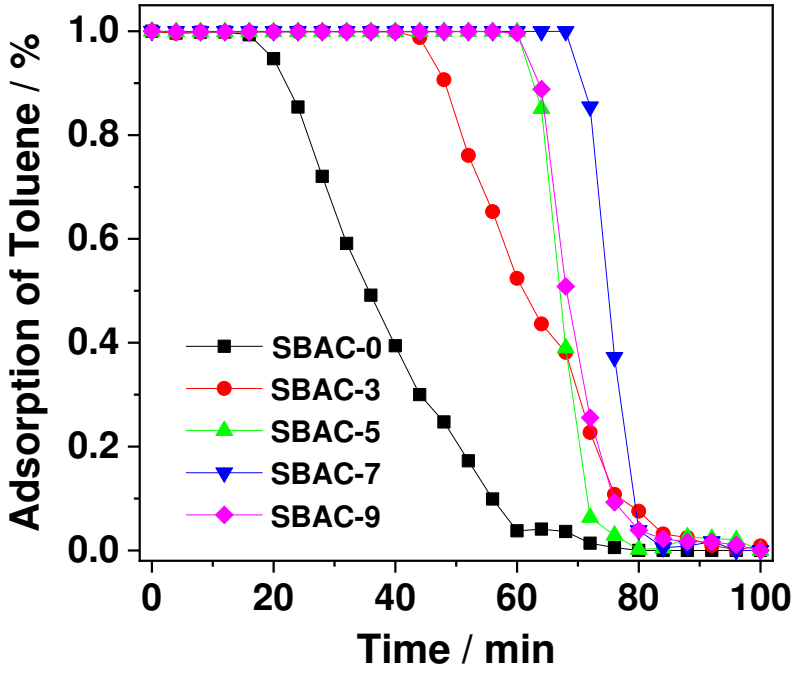
Adsorption of Toluene / %
1.0
0.8
0.6
0.4
0.2
0.0
0
20
40
60
80
100
Time / min
SBAC-0
SBAC-3
SBAC-5
SBAC-7
SBAC-9

Figure 7

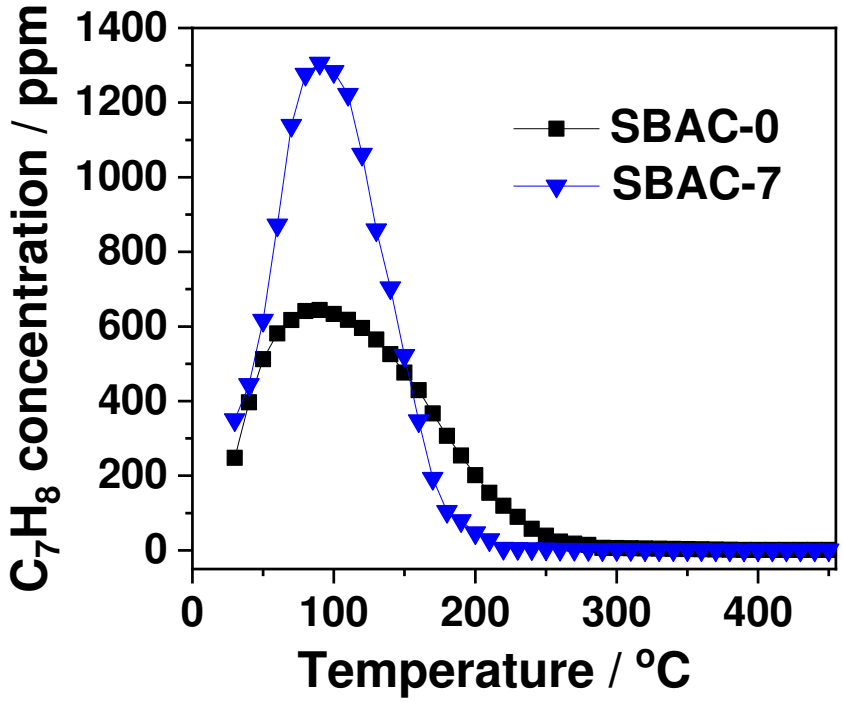
1400
1200
1000
800
600
400
200
0
0
100
200
300
400
C7H8 concentration / ppm
Temperature / °C
SBAC-0
SBAC-7

Figure 8

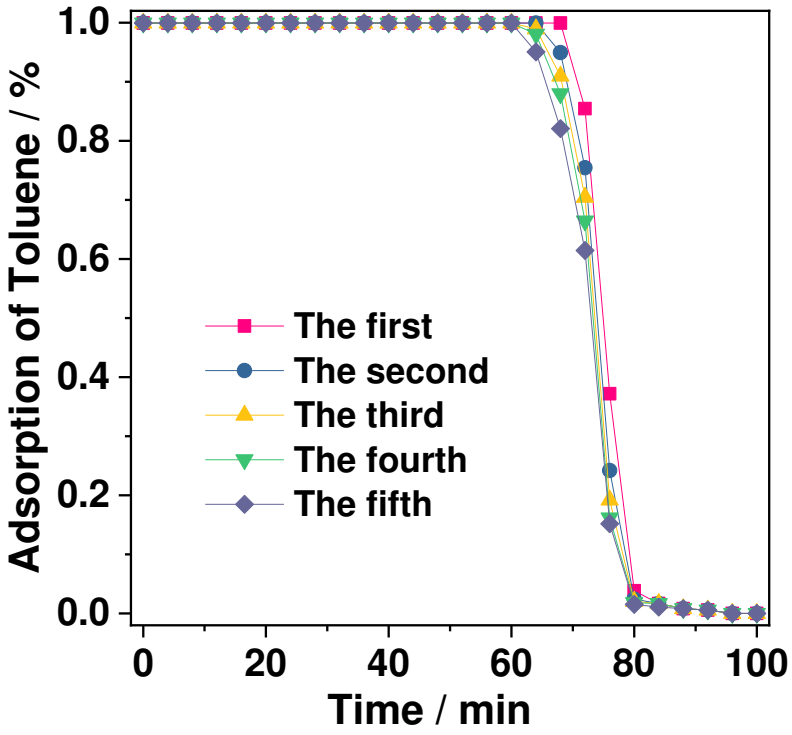
Adsorption of Toluene / %
1.0
0.8
0.6
0.4
0.2
0.0
0
20
40
60
80
100
Time / min
The first
The second
The third
The fourth
The fifth

Figure 9

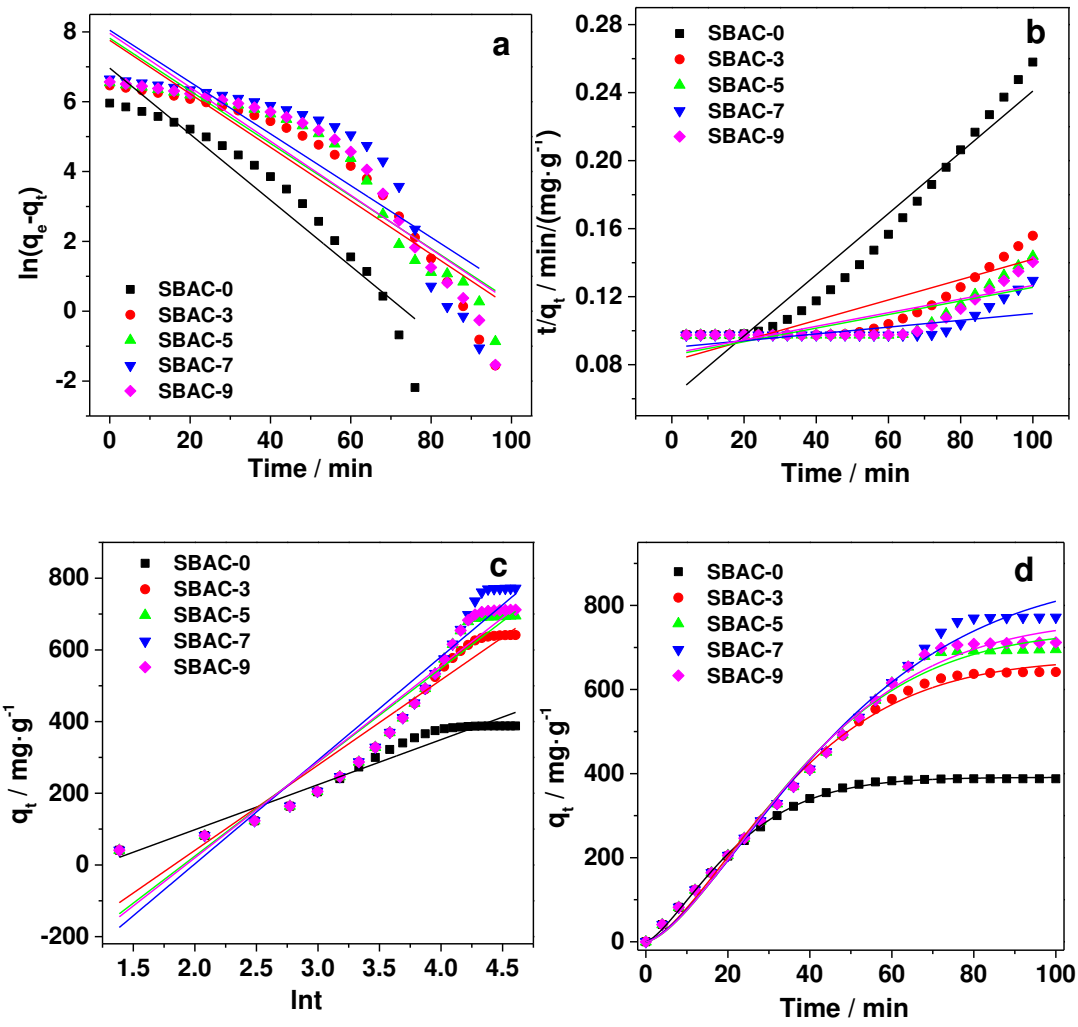
a
b
c
d
SBAC-0
SBAC-3
SBAC-5
SBAC-7
SBAC-9
ln(qe-qt)
Time / min
t/qt / min/(mg·g-1)
qt / mg·g-1
lnt

Figures

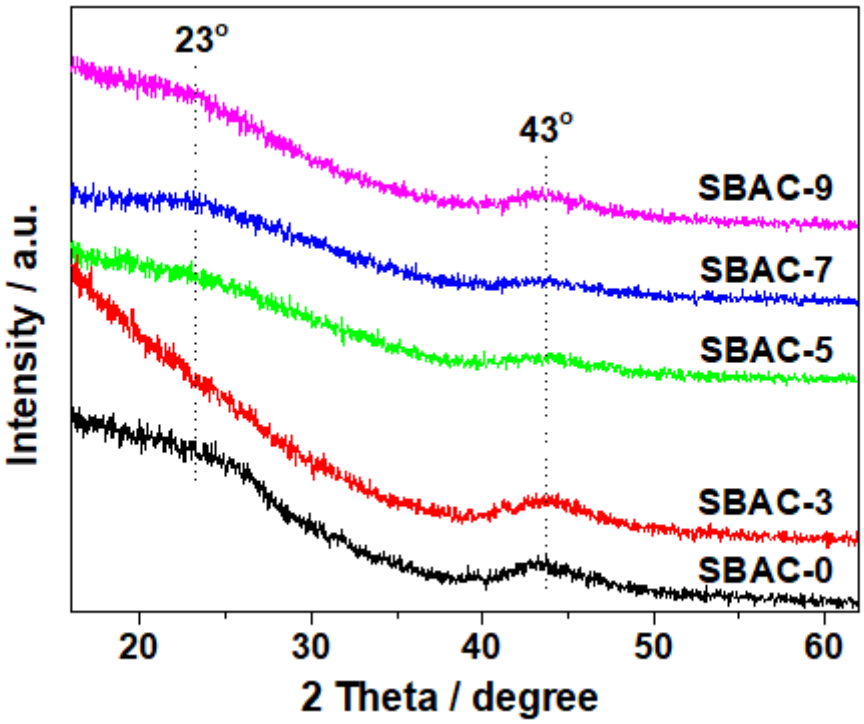

Figure 1

XRD patterns of the as-prepared samples.

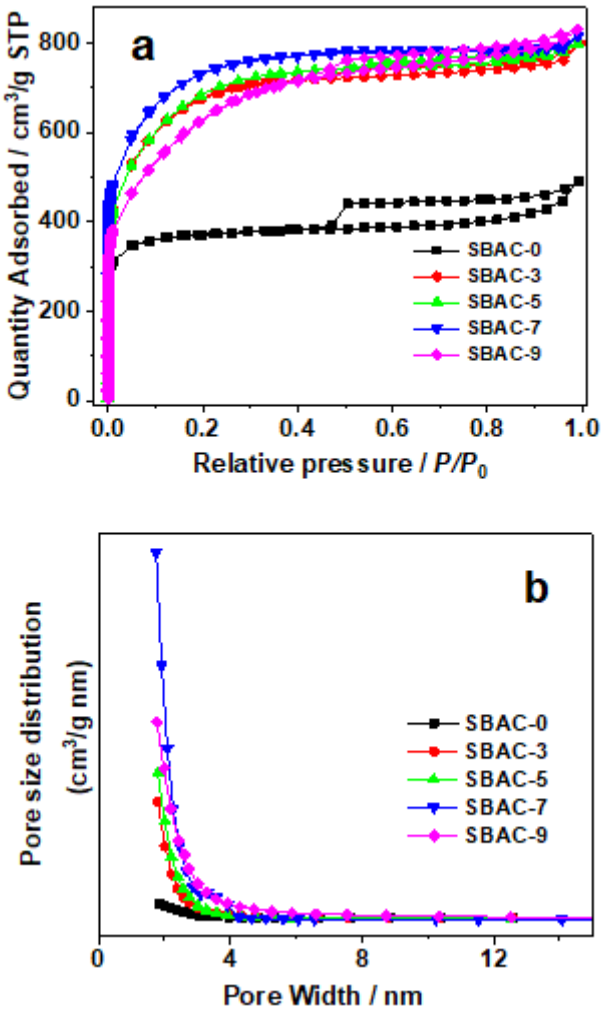

Figure 2

(a) N2 sorption isotherms and (b) pore-size distributions of the as-prepared samples.

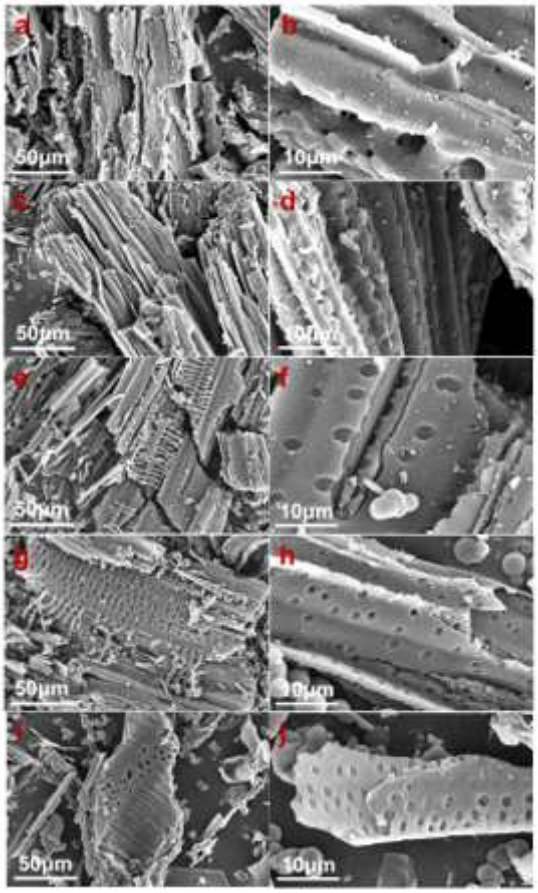

Figure 3

SEM images of as-prepared activated carbon samples SBAC-0 (a, b), SBAC-3 (c, d), SBAC-5 (e, f), SBAC-7 (g, h), and SBAC-9 (i, j).

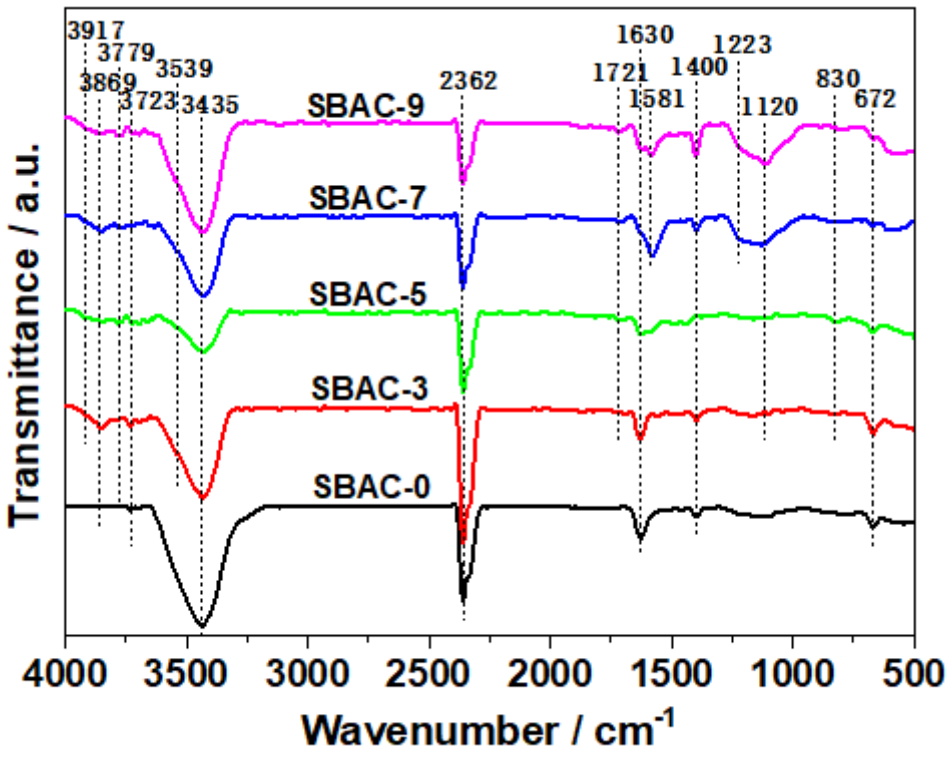

Figure 4

FT-IR spectra of the as-prepared samples.

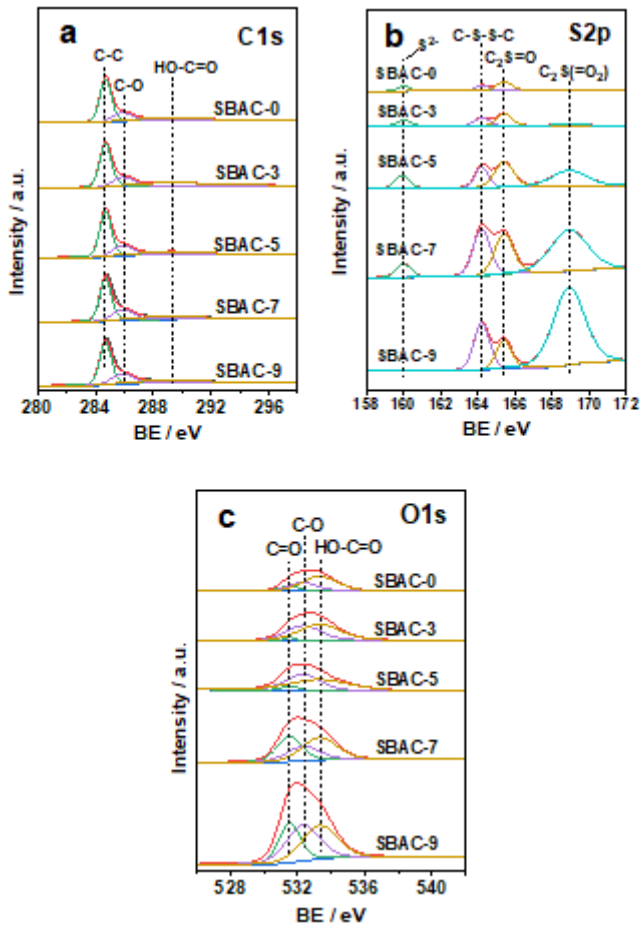

Figure 5

(a) C 1s, (b) S 2p and (c) O 1s XPS spectra of the as-prepared samples.

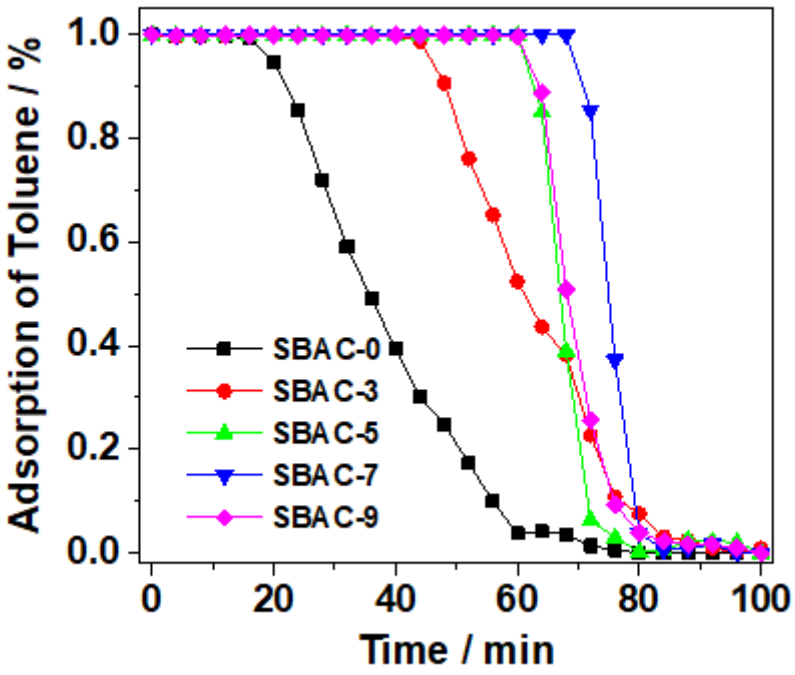

Figure 6

Adsorption breakthrough curves of as-prepared samples.

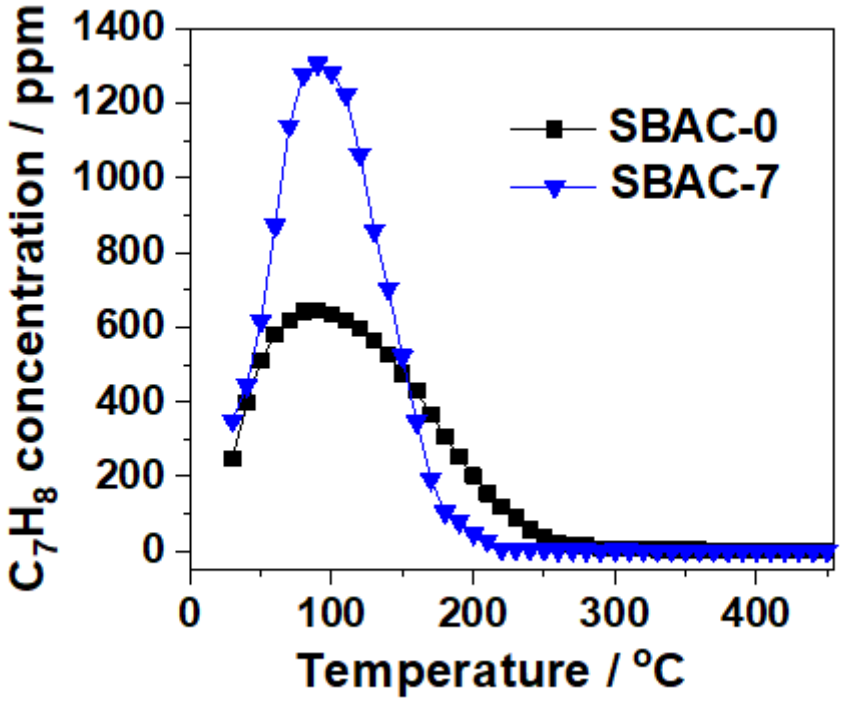

Figure 7

Desorption curves of SBAC-0 (a) and SBAC-7 (b).

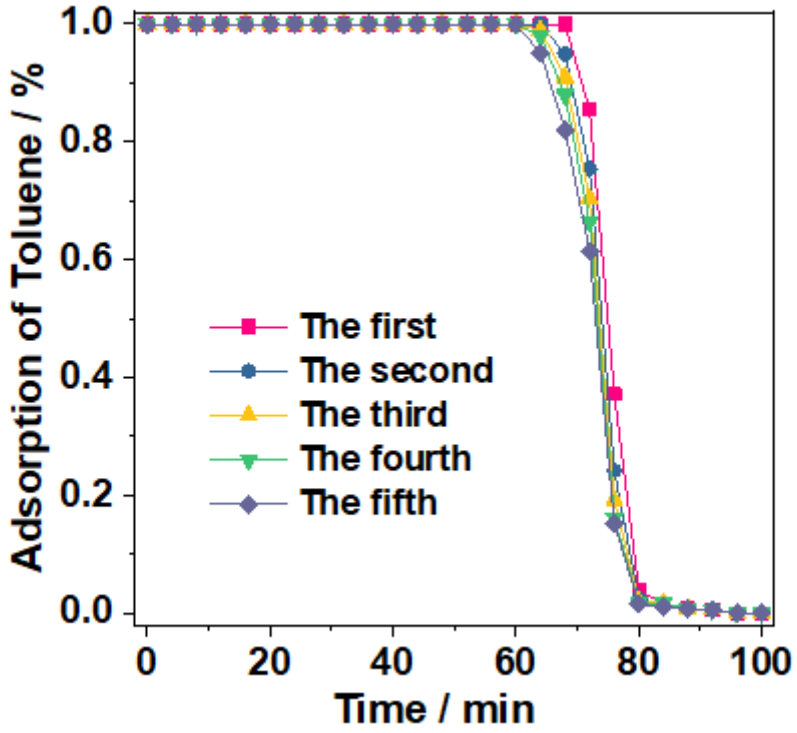

Figure 8

The consecutive toluene adsorption-desorption cycles of SBAC-7.

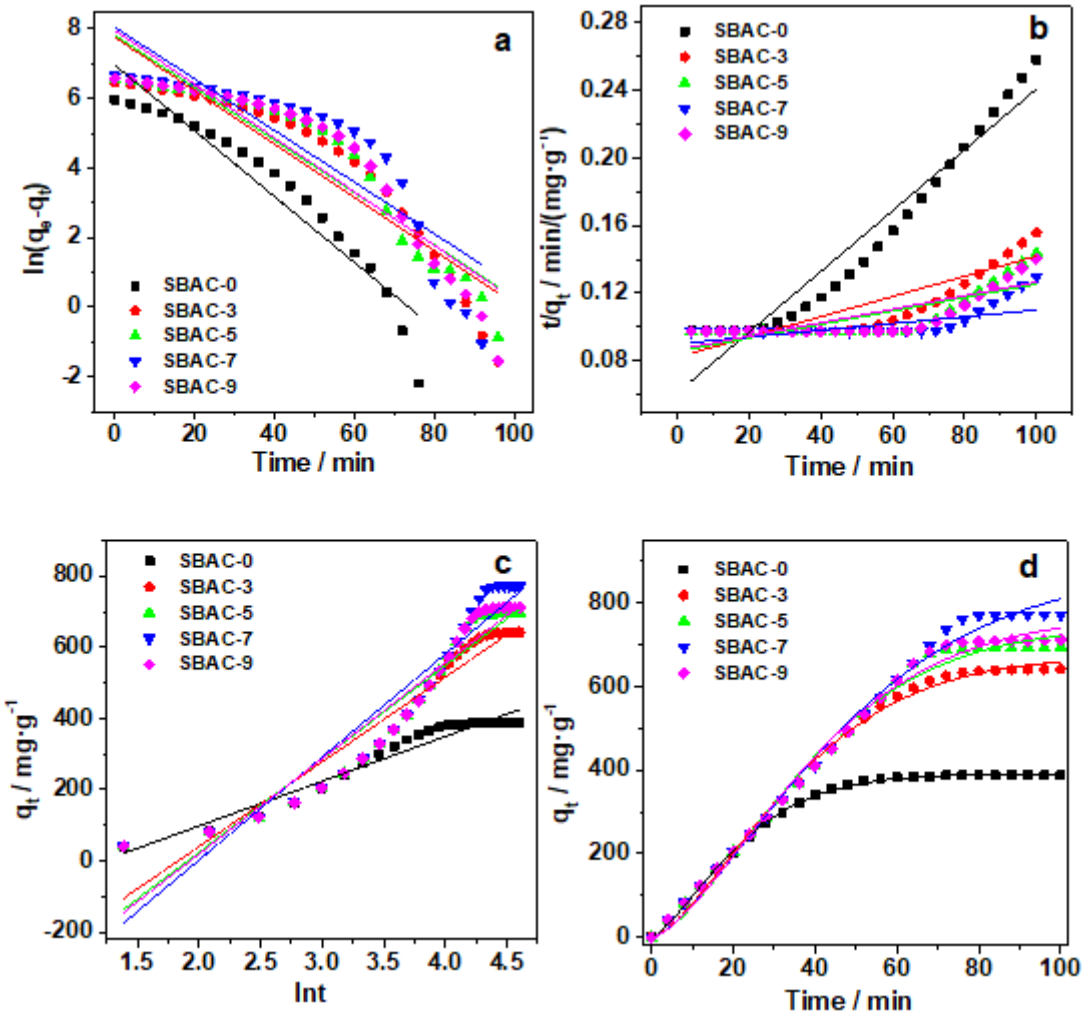

Figure 9

Adsorption kinetics model fit adsorption curve: (a) Pseudo-first-order model, (b) Pseudo-second-order model, (c) Elovich model, (d) Bangham model.